

Published in final edited form as:

J Colloid Interface Sci. 1999 December 1; 220(1): 163–169. doi:10.1006/jcis.1999.6524.

Atomic Force Microscopy and Wettability Study of Oxidized Patterns at the Surface of Polystyrene

Christine C. Dupont-Gillain^{*}, Bernard Nysten[†], Vladimir Hlady[‡], and Paul G. Rouxhet^{*1}

^{*}Unité de chimie des interfaces, Université Catholique de Louvain, Place Croix du Sud 2/18, B-1348 Louvain-la-Neuve, Belgium

[†]Unité de chimie et de physique des hauts polymères, Université Catholique de Louvain, Place Croix du Sud 2/18, B-1348 Louvain-la-Neuve, Belgium

[‡]Department of Bioengineering, University of Utah, Salt Lake City, Utah 84112

Abstract

The surface properties of patterned surfaces made by a combination of photolithography and oxygen plasma treatment of polystyrene (PS) were investigated. PS and plasma-treated PS (PS_{ox}) were first characterized using X-ray photoelectron spectroscopy and the study of wetting dynamics (Wilhelmy plate method) in water and in solutions of different pH. The results indicated that the PS_{ox} surface may be viewed as covered with a polyelectrolyte-like gel, which swells depending on pH. It was then shown, using atomic force microscopy (AFM), that the adhesion force measured on PS with a silicon tip in water was higher compared with that measured on PS_{ox}. This feature allowed imaging of the oxidation patterns using the adhesion mapping mode. The origin of the pulloff force contrast, which could not be explained by combining Johnson–Kendall–Roberts theory and thermodynamic considerations, was attributed to repulsion between the tip and hydrated polymer chains present on the oxidized surface. Imaging was also performed in the lateral force mode, a higher friction being recorded on PS than on PS_{ox}.

Keywords

atomic force microscopy; plasma treatment; polystyrene; Wilhelmy plate method; Johnson–Kendall–Roberts model; surface forces

INTRODUCTION

Polymer materials are often surface-treated to change the chemical composition, increase the surface energy, or modify the surface topography while keeping the bulk properties unchanged (1–3). Typical examples are the oxidation of polyolefins to improve paint adhesion (2) and the elaboration of biomaterials (4). The physical or chemical modifications may affect a surface layer over a depth varying from a few nanometers to tens of micrometers. Four regions may be considered: the surface as such, which determines the wetting properties and may be analyzed by time-of-flight secondary ion mass spectrometry (ToF-SIMS); the near surface, which is probed by X-ray photoelectron spectroscopy (~5 nm deep); the deeper region of modified polymer; and, finally, the native polymer (5).

The oxidation of the polystyrene surface using oxygen plasma has been extensively studied (6–12). Various oxygen-containing functions are introduced by the treatment, with a concomitant increase in hydrophilicity. The oxygen uptake of polystyrene on plasma treatment is higher compared with that of other polymers, due to its aromatic character (10, 11). *In situ* analysis revealed that part of the surface modification occurs after exposure of the samples to the ambient atmosphere (11). Etching of the polymer surface takes place together with functionalization (11); low-molecular-weight fragments are produced and may be removed by solvents (6–8). It appears that the molecular mobility of the polystyrene chains is enhanced by the plasma treatment (7). The surface of plasma-oxidized polystyrene undergoes reorganizations on aging, as a result of both diffusion and molecular motions (12). The driving force for these reorganizations is the surface free energy (6).

Compared with the techniques commonly used to characterize plasma-treated polymer surfaces, atomic force microscopy (AFM) (13) offers two important advantages: (i) the samples do not need to be put *in vacuo* and may even be characterized in a liquid environment, which is of great interest for biomaterials; (ii) the lateral resolution is in the range of a few nanometers. The high lateral resolution of AFM allows imaging of heterogeneous surfaces which may have applications in different fields (biomaterials, biosensors, etc.). It also provides an opportunity to analyze simultaneously nontreated and treated areas of a surface, which facilitates direct evaluation of the treatment-induced properties. While AFM is routinely used to image topographic features on surfaces, a challenge is to develop it into a physicochemical characterization tool (14). Deflection versus tip–sample separation curves may provide information on surface forces (14–16) and mechanical properties of surfaces (17); arrays of such curves allow mapping of the surface properties of heterogeneous samples (18–23). Lateral force microscopy (LFM) may also reveal heterogeneity of surface properties, a higher tip–sample adhesion leading to a higher friction force (24–28). Force–distance curves and LFM have already been used to investigate model patterned surfaces (self-assembled monolayers) (24, 25, 29–32). However, there have been few attempts to apply such an approach to the study of “real” polymer surfaces, i.e., materials of industrial origin, relevant to practical applications.

The aim of this work is to investigate the physicochemical properties of micrometer-sized oxidized tracks produced at the surface of polystyrene by means of a photolithographic method and plasma discharge. These surfaces have been successfully used to achieve a selective adsorption of extracellular matrix proteins on the tracks and, thereby, to confine the adhesion of mammalian cells (33–35). Polystyrene and oxygen plasma-treated polystyrene are characterized using X-ray photoelectron spectroscopy (XPS) and study of the wetting dynamics using the Wilhelmy plate method; patterned surfaces are imaged using AFM in different modes.

MATERIALS AND METHODS

1. Sample Preparation

The polystyrene (PS_{native} = PS_n) originated from Petri dishes (UV-sterilized, Merck–Belgolabo, Belgium). It was cleaned by ultrasonication in isopropanol (analytical grade, VEL, Belgium) and dried under a nitrogen flow. Micrometer-sized tracks (7 μm wide) of plasma-oxidized polystyrene (PS_{ox}) were made as described elsewhere (34). Briefly, a photosensitive resin was spin-coated on PS_n substrates; the resin was submitted to UV light irradiation through a mask; development led to dissolution of the exposed resin; the sample was then submitted to a cold plasma discharge in oxygen atmosphere; and, finally, the remaining resin was dissolved, leaving a polystyrene (PS) matrix exposed at the surface in alternation with PS_{ox} tracks. The plasma discharge was performed in a barrel reactor (Plasmafab 505 from ETA Electrotech) at a frequency of 60 kHz. Prior to oxygen

admission, the reactor chamber was evacuated down to a pressure of 9×10^{-5} bar. The treatment lasted 2 min at a power of 50 W, under an oxygen (>99.9999% pure from Air Liquide) flow leading to a working pressure of 7×10^{-4} bar.

Nonpatterned surfaces of PS and of PSox were also prepared following the method described above but without exposure to UV light and with exposure in the absence of a mask, respectively. Moreover, samples of oxidized PSn (PSnox) were prepared by direct treatment with oxygen plasma discharge.

2. Surface Characterization

X-ray photoelectron spectra were recorded using a SSX-100 spectrometer (Model 206 from Surface Science Instruments) equipped with a monochromatized aluminum anode (10 kV, 12 mA). The order of peak analysis was survey scan, C 1 s, O 1 s, N 1 s, and C 1 s again. No modification of the C 1 s peak shape under X-ray irradiation was noted, indicating that the samples did not undergo degradation during analysis (36). A Shirley-type nonlinear background subtraction was used (37). Intensity ratios were converted into atomic concentration ratios by using the sensitivity factors proposed by the manufacturer (Scofield photoemission cross sections, variation of the electron mean free path according to the 0.7 power of the kinetic energy, constant transmission function).

Wetting of the samples with water (purified by MilliQ Plus system from Millipore; pH 5.6) and with KOH (analytical grade, Janssen, Belgium, pH 11.0) and HNO₃ (analytical grade, Merck–Belgolabo; pH 3.0) 10^{-3} M solutions was investigated under dynamic conditions using the Wilhelmy plate method, with DCA 322 equipment from Cahn Instruments. The measurements were performed at room temperature. The water container was closed with a lid pierced with a small hole to ensure a relative humidity of 95% 1 cm above the water surface. Successive cycles of immersion and emersion (advancing–receding) were performed and the contact angle (θ_{adv} , θ_{rec}) was recorded. Therefore, the effect of buoyancy was corrected and the position was referred to the three-phase contact line as described before (38). The surface tension of the KOH and HNO₃ solutions was not significantly different from that of pure water. In certain cases, pauses were made between successive cycles.

3. AFM Examination

Force–distance curves were recorded on PS and PSox in water (doubly distilled or MilliQ) with two different AFM instruments (Explorer from Topometrix, Autoprobe CP from Park Scientific Instruments), using silicon tips integrated into triangular levers (Park Scientific Instruments, nominal spring constant = 0.16 or 0.24 N/m, expected radius of curvature of the tip = 10 nm). The levers were washed with hydrogen peroxide (UCB, Belgium) and rinsed with water just before use. The diode voltage versus sample displacement data were converted to force versus tip–sample separation (15).

Mapping of patterned polystyrene was performed using different imaging modes, with an Explorer AFM (Topometrix) using a silicon tip integrated into a triangular lever (Park Scientific Instruments, nominal spring constant = 0.16 N/m, washed as described here above). The scanner had an x – y range of 150 μm and a z range of 12 μm . All the observations were made in doubly distilled water. Height and lateral force images were acquired simultaneously at a scan rate of 2 lines/s. The images obtained by forward and backward scanning were both recorded. Adhesion mapping was performed by recording force–distance curves on a finite number of locations on the sample surface (50×50 points). The adhesion force was then extracted from each curve and a map of the surface was reconstructed on basis of the adhesion force.

RESULTS

Surface analysis by XPS revealed an increase in the O/C atomic concentration ratio as a result of plasma treatment, from 0.01 to 0.10 for PS and from less than 0.005 to 0.20 for PSn. The nitrogen signal was below the detection limit, except for PSnox. From the shape of the C 1s and O 1s peaks recorded on PSox and PSnox (results not shown), it can be inferred that oxygen incorporated by the plasma treatment is involved in various chemical functions including alcohol, carbonyl, and carboxyl groups. The N 1s peak of PSnox appeared at 401.5 eV and may be attributed to ammonium produced by chemi-sorption of atmospheric ammonia on acidic surface sites (39).

The variation of $\cos \theta$ during successive immersion–emersion cycles, measured by the Wilhelmy plate method in water, is shown in Fig. 1 for PS and PSox. θ_{adv} and θ_{rec} recorded during the first cycle are respectively 93° and 51° for PS and 41° and 0° for PSox. PSox is thus more hydrophilic than PS. PS shows a constant hysteresis loop on repeated wetting cycles. For PSox, $\cos \theta_{adv}$ remains close to 1 when a cycle is performed immediately after the previous one or after a pause of 5 min. When the emersed sample is submitted to a longer pause before starting a new cycle, $\cos \theta_{adv}$ shifts to the value observed during the first cycle and may even become smaller.

Figure 2 presents the variation of $\cos \theta$ measured on PSnox during successive immersion–emersion cycles in solutions of varying pH. The behavior at pH 3.0 and 5.6 shows the same trend as for PSox with water. However, at pH 3.0, $\cos \theta_{adv}$ measured after a pause shifts more readily to lower values compared with pH 5.6. At pH 11.0, $\cos \theta_{adv}$ remains close to the value of $\cos \theta_{rec}$ even after a pause of 30 min.

Representative force–distance curves acquired by AFM on PS and PSox in water are shown in Fig. 3. The adhesion force (F_{adh}) was taken as the pulloff force recorded on tip–sample separation (18), as indicated in Fig. 3. F_{adh} was measured in five independent experiments; two of them were performed with the Topometrix and the other three with the Park Scientific Instruments microscope. Whatever the experiment, F_{adh} was higher for PS than for PSox. The couple of values depended on the experiment, presumably due to the variability of the tip curvature radius (40). Couples of minimum F_{adh} measured were 7 and 0 nN for PS and PSox, respectively; couples of maximum values were 50 and 4 nN for PS and PSox, respectively. Moreover, while a jump-in-contact was observed on tip–sample approach on PS, it was absent on PSox.

Figure 4 presents AFM data recorded in water on the same zone of a patterned sample. Figure 4a shows a height image; the backward scanning of the same area gave an identical image except for a slight lateral shift (image not shown). The PSox tracks can be identified on the image as slightly darker, thus lower, regions, but the height difference between the PSox tracks and the PS matrix is small compared with the sample roughness. Advantage was taken of the F_{adh} difference between PS and PSox to image the same surface using adhesion mapping in water (Fig. 4b). There is a marked contrast between the tracks and the matrix, F_{adh} being lower on PSox than on PS. A histogram of the recorded F_{adh} is presented in Fig. 4c. It shows a bimodal distribution, with a mode centered on $F_{adh} = 18$ nN, representing high adhesion measured on PS, and the other, less precisely defined, representing low adhesion measured on PSox. The comparison between Figs. 4a and 4b shows that the topographic features of the surface have no significant influence on the magnitude of the recorded F_{adh} . The adhesion map thus gives an image of the surface that is independent of its topography and reflects the difference in physicochemical properties between the PS and the PSox phases.

Figure 5 presents AFM images of patterned polystyrene, recorded in the lateral force mode in the forward (Fig. 5a) and backward (Fig. 5b) directions. These images were obtained in water, simultaneously with the height image presented in Fig. 4a. The contrast indicates that higher lateral forces are sensed on the PS matrix compared with the PSox tracks. Comparison with the height image (Fig. 4a) indicates that the signal recorded in the lateral force mode is not significantly influenced by the sample surface topography. Moreover, the contrast reversal that occurs when the scanning direction is reversed demonstrates that the contrast between the tracks and the matrix is due to true friction and not to a topography-related artifact. Like the adhesion mapping mode, the lateral force mode thus produces images that are independent of the topography and are related to physicochemical properties of the sample surface.

DISCUSSION

PS and PSox show very different behavior on wetting (Fig. 1). The shape of the hysteresis loops recorded on PSox is strongly affected by a previous contact of the sample with water and is dependent on the duration of the pauses between the cycles. This particular shape may be explained by water retention occurring on the surface after the first immersion–emersion cycle: $\cos \theta_{adv}$ remains close to 1 as long as the surface is covered by a film of water; it decreases if the sample is allowed to dry between cycles. Water retention might tentatively be attributed to increased roughness or to pore formation following plasma treatment; however, this is not observed on the AFM height images.

To understand the origin of the water retention observed on PSox, wetting was studied on PSnox samples as a function of pH. The shape of the hysteresis loop is clearly pH dependent (Fig. 2), the water retention effect being more pronounced at higher pH values. Besides, XPS results show that carboxylic functions are introduced by the plasma treatment, and it has been shown, using streaming potential measurements, that the surface of oxygen plasma-treated polystyrene is more negatively charged compared with that of polystyrene (41).

From this information, it can be inferred that the PSox surface is covered by a polyelectrolyte. At high pH, the carboxylic functions are deprotonated, which provokes a repulsion between adjacent polymer chains; water penetrates between the chains and swells the surface which behaves like a hydrogel. As the pH decreases, the repulsion between macro-molecules decreases, resulting in less pronounced water retention by the surface. After a pause of 30 min, the surface remains hydrated at pH 11.0 while it is completely dried at pH 3.0; the behavior is intermediate at pH 5.6.

It was also observed that $\cos \theta_{adv}$ of oxidized polystyrene reaches lower values during cycles performed after long pauses, as compared with the first cycle (PSox in Fig. 1, PSnox at pH 3.0 in Fig. 2). This could be due to dissolution of functionalized polymer chains during the analysis. Low-molecular-weight fragments produced during oxygen plasma treatment (8, 42) may indeed be extracted by solvents. Another explanation could be that hydrophobic recovery (12) of the plasma-treated surface occurs during long pauses subsequent to wetting, due to reorientation or diffusion of functionalized polymer chains into the sample.

The F_{adh} difference measured between PS and PSox may be tentatively explained using surface energy considerations. This approach has been widely reported in the literature (14, 23, 25, 29) using the Johnson–Kendall–Roberts (JKR) (43) model which predicts that

$$F_{adh} = 1.5 \pi R W_{adh}, \quad [1]$$

where R is the radius of curvature of the AFM tip and W_{adh} is the work of adhesion. It was found here that W_{adh} is lower for PSox than for PS. At first sight, it fits the common sense that the work of adhesion under water is lower when the surface is more hydrophilic. However, the common sense tends to create confusion between the work of adhesion and the interfacial energy. In fact, the different interfacial energies involved in W_{adh} should be taken into consideration:

$$W_{adh} = \gamma_{sample,water} + \gamma_{tip,water} - \gamma_{tip,sample}. \quad [2]$$

This is equal to

$$W_{adh} = W_{tip,sample} - W_{sample,water} - W_{tip,water} + 2\gamma_{water}, \quad [3]$$

where $W_{tip,sample}$, $W_{sample,water}$, and $W_{tip,water}$ correspond to works of adhesion *in vacuo*. $W_{sample,water}$ and $W_{tip,water}$ may be deduced from water contact angles θ :

$$W_{sample,water} = \gamma_{water}(\cos\theta_{sample} + 1), \quad [4]$$

$$W_{tip,water} = \gamma_{water}(\cos\theta_{tip} + 1). \quad [5]$$

$W_{tip,sample}$ may then be determined combining Eqs. [1] and [3]. $W_{tip,PS}$ and $W_{tip,PSox}$ were evaluated using $\gamma_{water} = 72$ mN/m, F_{adh} and θ_{adv} given above for the samples, and $\theta_{tip} = 40^\circ$ as measured on a silicon wafer cleaned in the same way as the tip. This led to values of about 220 mN/m for $W_{tip,PS}$ and about 120 mN/m for $W_{tip,PSox}$, considering the announced tip curvature radius of 10 nm for the couples of minimum F_{adh} values and a radius of 50 nm for the couples of maximum values.

On the other hand, one may also write

$$W_{tip,sample} = \gamma_{tip,vacuum} + \gamma_{sample,vacuum} - \gamma_{tip,sample}. \quad [6]$$

As PSox and the silicon tip are hydrophilic and PS is hydrophobic, $\gamma_{sample,vacuum}$ is expected to be higher for PSox than for PS, while $\gamma_{tip,sample}$ is expected to be higher for PS than for PSox. This would lead to a higher value of $W_{tip,PSox}$ compared with $W_{tip,PS}$, which is in contradiction with the above predictions based on application of the JKR model to our experimental data.

This brings us to discuss the limitations of coupling the JKR model with a thermodynamic approach to adhesion phenomena:

- i. JKR theory assumes perfectly smooth surfaces (43, 44). This is not a severe limitation on soft materials where the deformation is so important that the influence of surface roughness is negligible (43). Model systems commonly used in AFM

studies, i.e., self-assembled monolayers, are also very smooth (25, 29). On the other hand, the system investigated here does not respond to this assumption as demonstrated by the AFM images and by the behavior of PSox on wetting.

- ii. Equations [4] and [5] are valid for rigid surfaces (44, 45). It is thus paradoxical to combine JKR theory, which accounts for the elastic deformation of surfaces, with these equations. In our particular case, Eq. [4] is questionable as it was shown that the PSox surface behaves like a gel in water.
- iii. Equations [4] and [5] were derived considering that γ_{sample} is the same *in vacuo* or in laboratory atmosphere, i.e., neglecting the spreading pressure π (45).
- iv. A thermodynamic approach supposes that reversible phenomena are taken into consideration. For many systems, contact angles are different on advancing or receding of the liquid on the surface; i.e., wetting is not reversible. In our particular case, PS and PSox indeed show hysteretic behavior on wetting and, moreover, the contact angle of PSox depends on previous contacts of the surface with water.

Moreover, real adhesion energies and adhesion energies computed from balances of surface free energies and contact angles may differ due to the contributions of surface–surface electrostatic interactions and steric repulsions. The F_{adh} difference observed in water between PS and PSox may then be explained considering the particular structure of PSox, i.e., the presence of a thin polyelectrolyte-like gel layer at the surface. This may be responsible for an electrostatic repulsion between the PSox surface and the tip. Even if the latter is not negatively charged, the highly hydrated macromolecular structure of PSox may lead to a repulsive contribution toward the AFM tip, due to steric repulsion. Steric repulsion occurs when polymer chains dangling in solution are compressed between two surfaces and results from a decrease in entropy associated with the confinement (44).

The lateral forces measured on PS were also higher than those measured on PSox; this allowed imaging of the tracks in the lateral force mode (Fig. 5). A friction contrast is often attributed to an elasticity difference between the phases, the AFM tip penetrating deeper into a softer surface, which results in more friction. This was identified as the basis of the friction contrast on lateral force images of phase-separated Langmuir–Blodgett films (30, 31). Due to its hydrogel-like character, the PSox surface is expected to be softer than the PS surface; accordingly, a higher friction would be expected on PSox than on PS. Actually, the contrary was observed. A first explanation is the decreased adhesion force existing between the hydrated PSox chains and the AFM tip, as a result of steric repulsion. It was indeed shown that friction was correlated either with F_{adh} (24) or with the adhesion hysteresis recorded between approaching and retracting force–distance curves (25–27). Moreover, a lower friction was measured on PS covered with PDMS than on PS and this difference was attributed to the high mobility of the PDMS chains (46). A second explanation, which is consistent with the former, is thus that the hydrated PSox chains are more mobile than the PS chains, which has been shown recently (7).

CONCLUSION

The results presented above show that, despite their roughness and their nonordered structure, patterned surfaces created by selective plasma treatment of polystyrene may be imaged in terms of their surface properties, using AFM in water, in the adhesion mapping mode and the lateral force mode. A higher adhesion, measured in a direction normal to the sample surface, is correlated with a higher friction, measured in a direction parallel to the sample surface.

The observed contrasts may be related to the changes in physicochemical properties induced by oxygen plasma treatment of polystyrene. The study of the wetting dynamics shows that the PSox surface may be considered as a polyelectrolyte-like gel, which swells according to pH. This highly hydrated macromolecular structure at the PSox surface induces repulsive interactions toward the AFM tip, leading to decreased adhesion and friction on PSox domains.

Acknowledgments

The authors thank Y. Adriaensen, A. Crahay, S. Derclaye, Y. Dufrene, M. Genet, G. Jogikalmah, and A. Pungor for technical assistance and fruitful discussions. The support from the National Foundation for Scientific Research (FNRS), of the Federal Office for Scientific, Technical and Cultural Affairs (Interuniversity Poles of Attraction Program), and from NIH Grant HL44538 is gratefully acknowledged.

References

1. Wu, S. *Polymer Interface and Adhesion*. Marcel Dekker; New York/Basel: 1982.
2. Brewis DM, Briggs D. *Polymer*. 1981; 22:7.
3. Fourche G. *Polym Eng Sci*. 1995; 35:968.
4. Hubbell JA. *Trends Polym Sci*. 1994; 2:20.
5. Ferguson, GS.; Whitesides, GM. *Modern Approaches to Wettability: Theory and Applications*. Schrader, ME.; Loeb, G., editors. Plenum; New York: 1992. p. 143
6. Murakami T, Kuroda S, Osawa Z. *J Colloid Interface Sci*. 1998; 202:37.
7. Murakami T, Kuroda S, Osawa Z. *J Colloid Interface Sci*. 1998; 200:192.
8. Schamberger PC, Abes JI, Gardella JA. *Colloids Surf B*. 1994; 3:203.
9. Hopkins J, Wheale SH, Badyal JPS. *J Phys Chem*. 1996; 100:14062.
10. Lianos L, Parrat D, Hoc TQ, Duc TM. *J Vac Sci Technol A*. 1994; 12:2491.
11. Petrat FM, Wolany D, Schwede BC, Wiedmann L, Benninghoven A. *Surf Interface Anal*. 1994; 21:402.
12. Occhiello E, Morra M, Garbassi F, Johnson D, Humphrey P. *Appl Surf Sci*. 1991; 47:235.
13. Binnig G, Quate CF, Gerber Ch. *Phys Rev Lett*. 1986; 56:930. [PubMed: 1003323]
14. Colton RJ, Barger WR, Baselt DR, Corcoran SG, Koleske DD, Lee GU. *J Adh Sci Technol*. in press.
15. Ducker WA, Senden TJ, Pashley RM. *Langmuir*. 1992; 8:1831.
16. Burnham NA, Colton RJ, Pollock HM. *Nanotechnology*. 1993; 4:64.
17. Hoh JH, Schoenenberger C-A. *J Cell Sci*. 1994; 107:1105. [PubMed: 7929621]
18. Mizes HA, Loh K-G, Miller RJD, Ahuja SK, Grabowski EF. *Appl Phys Lett*. 1991; 59:2901.
19. Radmacher M, Fritz M, Cleveland JP, Walters DA, Hansma PK. *Langmuir*. 1994; 10:3809.
20. Baselt DR, Baldeschwieler JD. *J Appl Phys*. 1994; 76:33.
21. van der Werf KO, Putman CA, de Groot BG, Greve J. *Appl Phys Lett*. 1994; 65:1195.
22. Cappella B, Baschieri P, Frediani C, Miccoli P, Ascoli C. *Nanotechnology*. 1997; 8:82.
23. Jogikalmath G, Stuart JK, Pungor A, Hlady V. *Colloids Surf A*. 1999 in press.
24. Frisbie CD, Rozsnyai LF, Noy A, Wrighton MS, Lieber CM. *Science*. 1994; 265:2071. [PubMed: 17811409]
25. Noy A, Frisbie CD, Rozsnyai LF, Wrighton MS, Lieber CM. *J Am Chem Soc*. 1995; 117:7943.
26. Marti A, Hähner G, Spencer ND. *Langmuir*. 1995; 11:4632.
27. Chaudhury MK, Owen MJ. *Langmuir*. 1993; 9:29.
28. Yoshizawa H, Chen Y-L, Israelachvili J. *J Phys Chem*. 1993; 97:4128.
29. van der Vegte EW, Hadziioannou G. *Langmuir*. 1997; 13:4357.
30. Green J-BD, McDermott MT, Porter MD, Siperko LM. *J Phys Chem*. 1995; 99:10960.
31. Overney RM, Meyer E, Frommer J, Güntherodt H-J, Fujihira M, Takano H, Gotoh Y. *Langmuir*. 1994; 10:1281.

32. Dufrêne YF, Barger WR, Green J-BD, Lee GU. *Langmuir*. 1997; 13:4779.
33. Dewez, J-L.; Lhoest, J-B.; Detrait, E.; Rouxhet, PG.; Bertrand, P.; Van Den Bosch De Aguilar, P. International Patent Application. PCT/BE/00104.
34. Lhoest J-B, Detrait E, Dewez J-L, van den Bosch de Aguilar P, Bertrand P. *J Biomater Sci Polym Educ*. 1996; 7:1039.
35. Dewez J-L, Lhoest J-B, Detrait E, Berger V, Dupont-Gillain CC, Vincent L-M, Schneider Y-J, Bertrand P, Rouxhet PG. *Biomaterials*. 1998; 19:1441. [PubMed: 9794515]
36. Dengis PB, Gerin PA, Rouxhet PG. *Colloids Surf B*. 1995; 4:199.
37. Shirley DA. *Phys Rev B*. 1972; 5:4709.
38. Tomasetti E, Rouxhet PG, Legras R. *Langmuir*. 1998; 14:3435.
39. Changui C, Doren A, Stone WEE, Mozes N, Rouxhet PG. *J Chim Phys*. 1987; 84:275.
40. DeRose JA, Revel J-P. *Microsc Microanal*. 1997; 3:203.
41. Rouxhet PG, Doren A, Dewez J-L, Heuschling O. *Progr Organic Coatings*. 1993; 22:327.
42. Callen BW, Ridge ML, Lahooti S, Neumann AW, Sohdi RNS. *J Vac Sci Technol A*. 1995; 13:2023.
43. Johnson KL, Kendall K, Roberts AD. *Proc R Soc London A*. 1971; 324:301.
44. Israelachvili, J. *Intermolecular and Surface Forces*. 2. Academic Press; London: 1992.
45. Andrade, JD.; Smith, LM.; Gregonis, DE. *Surface and Interfacial Aspects of Biomedical Polymers*. Andrade, JD., editor. Vol. 1. Plenum; New York/London: 1985. p. 249
46. Brown HR. *Science*. 1994; 263:1411. [PubMed: 17776511]

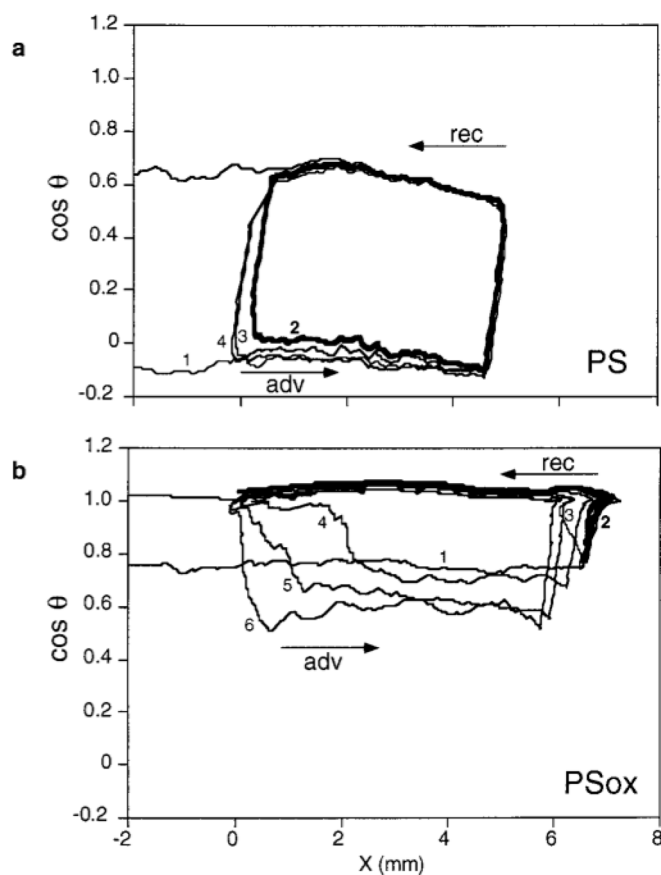


FIG. 1. Variation of $\cos \theta$ of water as a function of the three-phase contact line position X during successive immersion–emersion cycles for PS (a) and PSox (b), recorded without pause (cycle 2) or with a pause (5 min, 30 min, 2 h, and 10 h, before cycles 3, 4, 5, and 6, respectively).

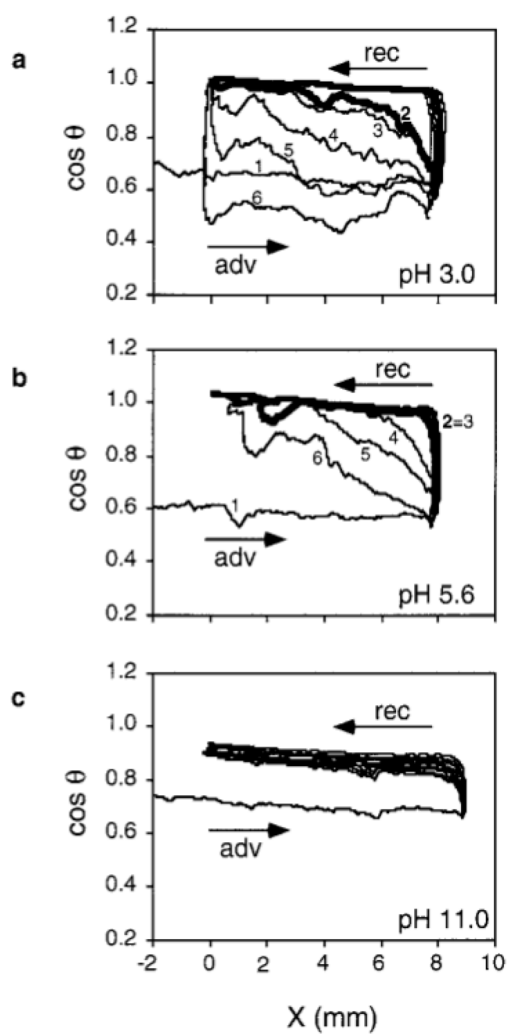


FIG. 2. Variation of $\cos \theta$ as a function of the three-phase contact line position X during successive immersion–emersion cycles on PSnox at pH 3.0 (a), 5.6 (b), and 11.0 (c), recorded without pause (cycles 2 and 3) or with a pause (5, 10, and 30 min before cycles 4, 5, and 6, respectively).

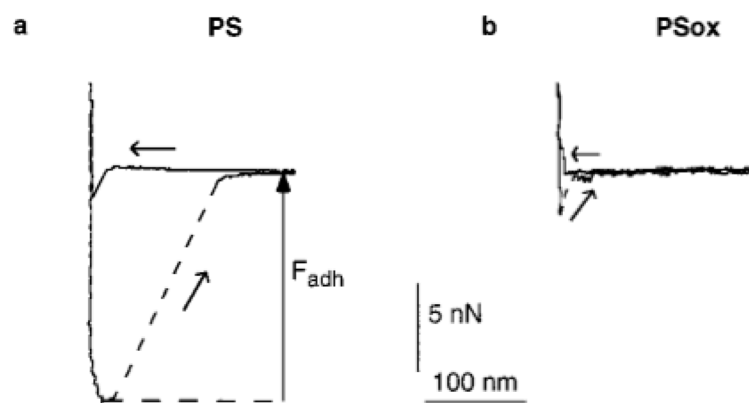


FIG. 3. Force measured between a silicon tip and PS (a) or PSox (b) in water, as a function of the tip-sample distance. Curves obtained on approach (\leftarrow) and separation (\nearrow) are presented.

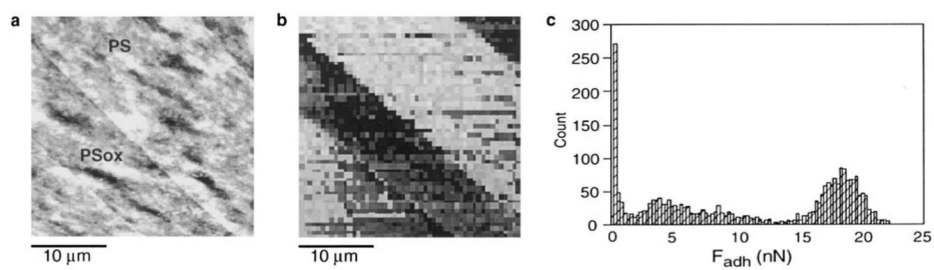


FIG. 4. AFM data recorded in water on the same zone of patterned polystyrene: (a) height image (forward scanning direction, vertical gray scale = 30 nm); (b) adhesion map (vertical gray scale = 25 nN); (c) histogram of the F_{adh} recorded in (b).

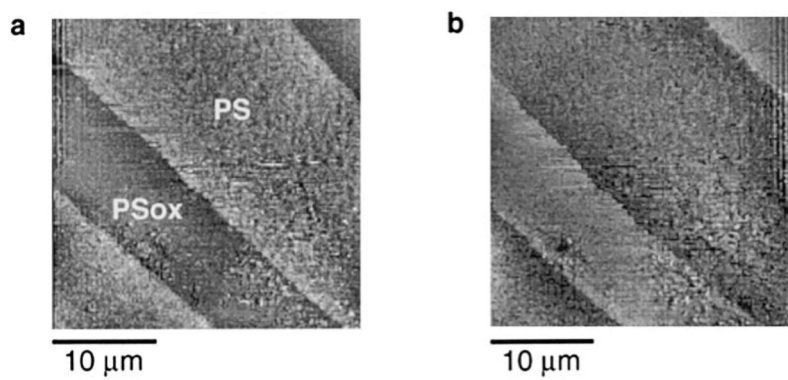


FIG. 5. AFM images recorded in water in the lateral force mode on patterned polystyrene, simultaneously with the height mapping shown in Fig. 4a: (a) forward scanning direction, (b) backward scanning direction.